



Seismic velocity imaging of the Kumaon–Garhwal Himalaya, India

Prantik Mandal¹ · D. Srinagesh¹ · R. Vijayaraghavan¹ · G. Suresh¹ · B. Naresh¹ · P. Solomon Raju¹ · Aarti Devi¹ · K. Swathi¹ · Dhiraj K. Singh¹ · D. Srinivas¹ · Satish Saha¹ · M. Shekar¹ · A. N. S. Sarma¹ · YVVBSN Murthy¹

Received: 1 August 2021 / Accepted: 24 November 2021 / Published online: 5 January 2022
© The Author(s), under exclusive licence to Springer Nature B.V. 2021

Abstract

Since the initial collision at 55 Ma, rocks of the Indian crust below the Himalayas have undergone modification chemically and compositionally due to the ongoing India–Asia convergence. The local earthquake tomography images a shallow ($\sim 1\text{--}2^\circ$) north-east-erly dipping low-velocity layer (10–20% drop in V_p and V_s , 10–15% increase in V_p/V_s) beneath the region between 10 and 20 km depth, which is inferred as the main Himalayan thrust (MHT). The presence of this low-velocity layer may be attributed to the presence of aqueous/metamorphic fluids or high fluid pressure, which may trigger crustal earthquakes by lowering the frictional coefficient ($\sim 0.01\text{--}0.08$) on the MHT. The 1803 $M_w 8.2$ Garhwal, 1991 $M_w 6.8$ Uttarkashi and 1999 $M_w 6.4$ Chamoli earthquakes have also been modelled to be triggered on the MHT, by the presence of aqueous/metamorphic fluids or high pore-fluid pressure. Besides, our modelling predicts three un-ruptured similar low-velocity zones on the MHT for generating future moderate to large fluid-triggered earthquakes in the region. The mapped low-velocity anomalies at 25–35 km depths further support the idea of the presence of a relatively higher temperature due to the hotter mantle below, which induces ductile rheology that prevents the lower crustal seismicity.

Keywords Local earthquake tomography · Main Himalayan thrust · Seismic velocity · V_p/V_s ratio · Rheology · Crust

1 Introduction

The mighty Himalaya represents the site for the active continent–continent collisional zone in the world and was formed through the formation of three major north-dipping thrusts since the initial collision between the Indian and Eurasian plates at 55 Ma (viz., youngest southernmost main frontal thrust (MFT), main boundary thrust (MBT) and main central thrust (MCT)) (Valdiya 1980). These thrusts root into a regional decollement or bed-parallel fault, representing the contact between the Indian and Eurasian plates (Seeber and

✉ Prantik Mandal
prantikmandal62@gmail.com

¹ CSIR-National Geophysical Research Institute, Uppal Road, Hyderabad, India

Armbruster, 1971). This decollement surface, which underlies the entire Himalaya, is more popularly known as the main Himalayan thrust (MHT). This has been the plane of occurrence for most of the moderate to great Himalayan earthquakes (Seeber and Armbruster, 1971). The geometry of the MHT has been imaged in terms of change in seismic velocities, lithologic changes, intense micro-seismicity, high electrical conductivity and focal depths of moderate earthquakes (Ni and Barazangi 1984; Na'b'elek et al. 2009; Caldwell et al. 2013; Schulte-Pelkum et al. 2005; Pandey et al. 1995; Lemonnier et al. 1999). A ramp in MHT is also inferred based on the clustering of micro-seismicity in the Nepal Himalaya (Pandey et al. 1995) and geological mapping as well as structural data in Garhwal Himalaya (Srivastava and Mitra, 1994). Recently, the double-difference tomography using P- and S- arrival times from the 2015 Gorkha aftershock sequence has imaged lateral variation of the low-velocity MHT zone between 15 and 30 km depths, which has been inferred to control the rupture length of the Gorkha earthquake (Bai et al. 2019). Nevertheless, the causative factors for earthquake generation associated with the MHT remain undetermined, which provides the required impetus to carry out a detailed local earthquake tomographic inversion of the Uttarakhand Himalayan region, to delineate the fine 3-D crustal seismic velocity structure of the Himalayan collision front including the geometry of MHT.

Prior to the occurrence of the 2015 Gorkha earthquake, the earthquake generation model of moderate to great Himalayan earthquakes was mainly constrained by pre-twentieth century felt-intensity reports, some recent instrumental seismological data and paleoseismological evidence of some great earthquakes (Seeber and Armbruster 1981; Ni and Barazangi 1984; Rajendran and Rajendran 2005). This scenario has been changed for the first time through modelling of instrumental data gathered during the 2015 Gorkha earthquake, which provided a better constrained model of earthquake generation on the north-dipping main Himalayan thrust (MHT) between 15 and 30 km depths, due to the high pore fluid pressure and continued convergence between the Indian plate and southern Tibet (Bai et al. 2019; Elliott et al. 2016). Several earlier studies using poorly constrained instrumental seismic data have also been imaged the geometry of the MHT in terms of change in seismic velocities, lithologic changes, intense micro-seismicity, high electrical conductivity and focal depths of moderate earthquakes (Ni and Barazangi 1984; Caldwell et al. 2013; Schulte-Pelkum et al. 2005; Pandey et al. 1995; Lemonnier et al. 1999). Nevertheless, the causative factors for earthquake generation associated with the MHT remain undetermined, which provides the required impetus to carry out a detailed local earthquake tomographic inversion of the Uttarakhand Himalayan region, to delineate the fine 3-D crustal seismic velocity structure of the Himalayan collision front including the geometry of MHT.

Until today, many damaging $M > 7$ earthquakes including at least four M8 great earthquakes have occurred along the 2500-km Himalayan frontal arc. However, the Kumaon–Garhwal Himalaya has been unique to experience repeated great earthquakes in 1505 and 1803. Considering a GPS-derived convergence rate of 15 mm/yr, Bilham (2019) has inferred an accumulated slip deficit of 3 m in the KG Himalaya, since the occurrence of 1803 event. Occurrences of the 1991 Uttarkashi and 1999 Chamoli earthquakes were not sufficiently large to release 3-m slip deficit. Thus, the occurrence of an earthquake of M7.3 is required to release the complete slip deficit in the Kumaon–Garhwal (KG) Himalaya (Bilham 2019). Based on the results from seismological, GPS and geological studies, it has now been established that the central GAP area in Himalaya (the region between the 1905 Kangra and 1934 Nepal–Bihar source region) is the locale for the future large M7 earthquakes in the Himalayan frontal arc (Bilham 2019; Vorobieva et al. 2017) and hence, it is necessary to monitor the earthquake activity in the central GAP area. The CSIR-National Geophysical Research Institute (CSIR-NGRI), Hyderabad, has been operating a regional

network of 56 three-component broadband stations in the Uttarakhand Himalayan region (Fig. 1a), since 2017, which provided the impetus to map (if any) the seismogenic volume for velocity variation and its correlation with earthquake generation in the KG Himalaya. In this paper, we present a 1D reference velocity model of the region, derived from a selected set of seismograms generated by 913 well-distributed earthquakes, with azimuth gaps $< 180^\circ$. This 1-D velocity model is derived by averaging 1-D Vs models obtained from the Differential Evolution waveform inversion of PRFs at 9 broadband stations within the MCT Zone (i.e. the region between Vaikrita (VT) and Munsiri (MT) thrusts) and region just south of it (Fig. 1a; “additional figures are given in Online Resource 1”) and used as a priori information to map the 3-D Vp and Vs variations within the study region using local earthquake tomography, by using 14,074 P- and 13,013 S- arrivals of 913 local earthquakes from a total of 65 broadband stations (Figs. 1a-d, 2a-c, 3a-e; “additional table is given in Online Resource 8”). Our tomographic images clearly map several important geological crustal features in the Uttarakhand Himalaya (Figs. 4–6 and “additional figures are given in Online Resources 2–4”).

2 Geology, tectonics and seismicity of the Kumaon–Garhwal Himalaya

Four major thrust fault systems (viz. Himalayan frontal thrust (HFT), main Boundary thrust (MBT), main Central thrust (MCT), and South Tibetan detachment (STD)) characterize the tectonics of the Kumaon and Garhwal Himalayas, wherein MFT separates Shivalik Himalayas (SH) from Indo-Gangetic plain, while MBT bounds Lower Himalayas (LH) in the south and higher Himalaya (HH) in the north (Fig. 1a) (Valdiya 1980; Seeber and Armbruster 1981; Ni and Barazangi 1984; Na’b’elek et al. 2009; Caldwell et al. 2013; Schulte-Pelkum et al. 2005; Pandey et al. 1995; Lemonnier et al. 1999; Srivastava and Mitra, 1994). The higher Himalaya (HH) is also separated from the LH by the MCT. And, the ITSZ (Indo-Tsangpo suture zone) is separated from the HH by the STD. In the Uttarakhand Himalaya, the MCT zone comprises two faults viz., Munsiri (MT) and Vaikrita (VT) (Valdiya 1980). Additionally, the Ramgarh thrust (RT) and Ton thrust (TT) are also present in the Lesser Himalaya. These major thrusts connect to a low-angle north-dipping plane at a depth, which is probably decoupled the Indian plate from the overriding Eurasian plate (Fig. 1b). Modelling of GPS data revealed that presently MHT is accommodating about 90% of strain energy resulting from the convergence between Indian and Eurasian plates (Bilham, 2019; Ader et al. 2012). Available fault plane solutions of earthquakes suggest the involvement of a low-angle north-dipping thrust fault for generating these events (Jain and Chander 1995; Kayal et al. 2003).

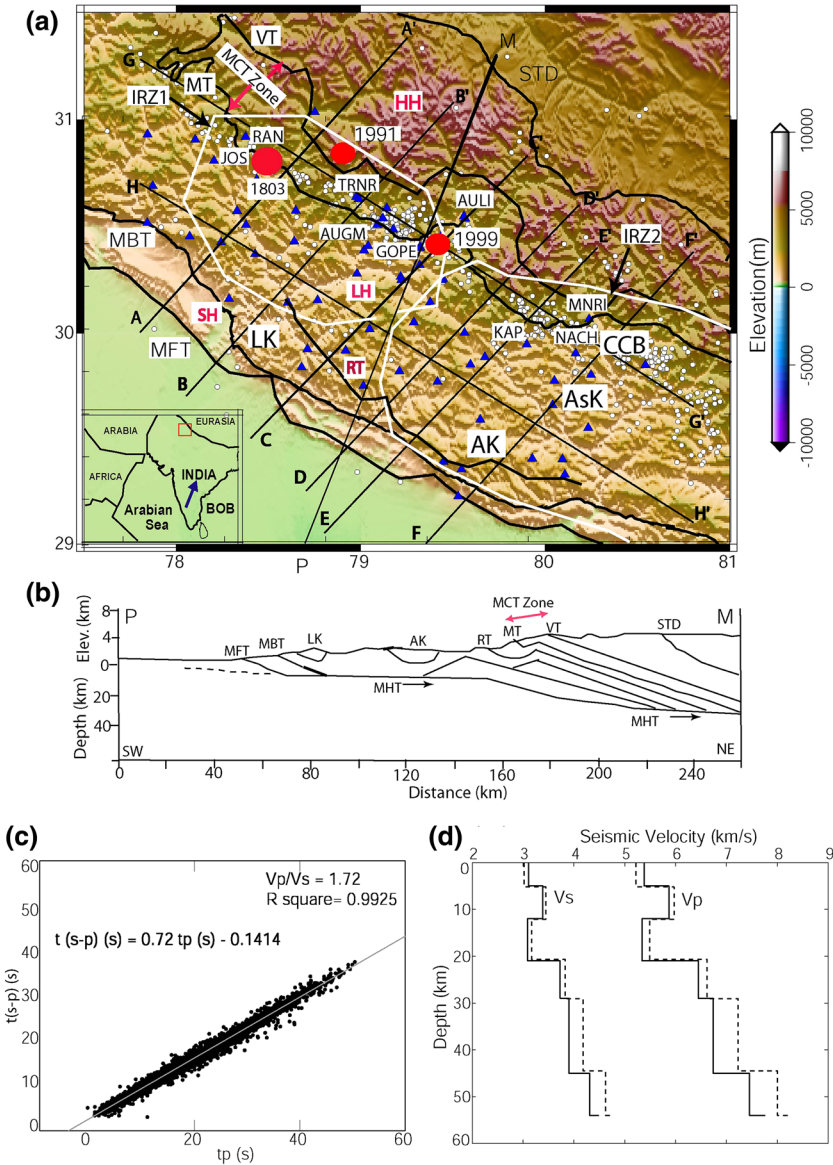
Occurrences of four great $M \geq 8$ (viz., 1505 Central Himalaya, 1897 Shillong, 1950 Assam, and 1934 Bihar–Nepal earthquakes) and three large $M7.5$ – 7.9 (viz., Kangra, 1905, $M7.8$, Kashmir, 2005, $M7.6$, and Nepal, 2015, $M7.8$) earthquakes in the past define the level of earthquake hazard associated with the Himalaya (Rajendran and Rajendran 2005; Bilham 2019; Vorobieva et al. 2017; Gupta and Gahalaut 2014). Besides, the seismic potential of the NW Himalaya has been manifested by the occurrences of several $M \geq 6$ earthquakes (e.g. the 1344 $M \geq 8$, 1505 $M8.2$ Lo Mustang, 1803 $M7.7$ Garhwal, 1905 $M7.8$ Kangra, 1975 $M6.8$ Kinnaur, 1991 $M6.8$ Uttarkashi and 1999 $M6.4$ Chamoli) (Rajendran and Rajendran 2005). Interestingly, most of these moderate to large earthquakes have occurred on the MHT (Bilham 2019), which has also been inferred from the geological data (Srivastava and Mitra 1994), seismological data (Caldwell et al. 2013) and GPS data

Fig. 1 **a** Station location map of the Uttarakhand region. Filled blue triangles mark the location of broadband stations, while small filled white circles mark the earthquake relocations obtained from simultaneous inversion. Solid black lines mark six profiles across the strike (AA', BB', CC', DD', EE', and FF') and two profiles along the strike (GG' and HH') of the collisional zone. The inferred rupture zones of the 1803 (IRZ1) and 1505 (IRZ2) earthquakes are marked by solid thick white lines (after Bilham (2019)). The solid black line represents faults. MT: Munsiri Thrust; VT: Vaikrita thrust; MZ: MCT Zone; RT: Ramgarh Thrust; TT: Ton Thrust; MBT: Main Boundary Thrust; MFT: Main Frontal Thrust; AsK: Askot Klippe; CCB: Chiplakot crystalline belt; LK: Lansdown Klippe; AK: Almora Klippe. Medium size red filled circles mark the epicentral locations of the 1991 M_w 6.8 Uttarakhand and 1999 M_w 6.4 Chamoli earthquakes, while a large red filled circle marks the location of the 1803 event. Inset shows the Indian plate and surrounding major plate boundaries. A red square marks the study area, while BOB marks the Bay of Bengal, **b** Schematic tectonic depth cross- $Sect.$ ¹ across the NE-SW trending profile PM, whose location is shown in Fig. 1a, **c** A Wadati plot of P-arrivals and (S-P) times of all the events used here, and **d** Final 1-D V_p and V_s models (shown by black dotted lines) determined from the simultaneous inversion of P- and S- arrival times of 923 local events from 10–35 stations, while initial velocity models are shown by solid black lines

(Bilham 2019). Several researchers have attributed the Kumaon–Garhwal (K-G) Himalayan seismicity to a zone parallel to the MCT lying between Yamuna and Alaknanda valleys (Gaur et al. 19,865; Khattri et al. 1989; Mandal et al. 2001). However, Yadav et al. (2009) showed the K-G Himalaya seismicity clusters close to the MCT. The confinement of micro-seismicity along the MBT has also been reported for the Kangra–Chamba earthquake region (Kumar et al. 2009), while the Kinnaur seismicity has been reported to be associated with the South Tibetan detachment (STD) and Kaurik–Chango fault (Joshi et al. 2010; Molnar and Lyon-Caen, 1989). Several micro-earthquake studies in Himalaya have been carried out in the recent past by operating various seismic networks (Pandey et al. 1995; Kumar et al. 2009; Monsalve et al. 2006; Langin et al. 2003; Drukpa et al. 2006) and the significant observation from these studies is the clustering of seismicity to the south of the MCT surface trace. In general, most of the Himalayan earthquakes are upper crustal in nature and are occurring on the north-dipping MHT. However, in Bhutan Himalaya earthquakes are located in the middle and lower crust (Drukpa et al. 2006), but lower crustal earthquakes are not present beneath the Nepal Himalayan segment (Pandey et al. 1995; Monsalve et al. 2006; Langin et al. 2003).

3 Data and methods

Here, we use P- and S- arrival times of 713 local earthquakes (M_L 0.8–5.6), which have been recorded by a close broadband seismic network of 56 three-component seismographs during 2017–2020 in Uttarakhand Himalaya that has been deployed by our Institute (Figs. 1a, 2a, 3a). We also add arrival times of 200 aftershocks (M_w 1.0–4.8) of the 1999 Chamoli earthquake from a local seismic network of nine 3-component broadband seismographs deployed by our Institute in 1999 (Mandal et al. 2001). Thus, we use 14,074 P- and 13,013 S-wave high-quality arrival times picked from the three-component seismograms of 913 events for our local earthquake tomography study (see Supplementary Table S1 online). The locations of these earthquakes are shown in Fig. 1a, while Fig. 2a–c shows an excellent sampling of the study region by rays suggesting a good coverage for our local earthquake tomography study. We obtained an average crustal V_p/V_s ratio of 1.72 for the region, through a Wadati plot of P-arrivals and (S-P) times of all the events (Fig. 1c). For the relocations of earthquakes, we use an initial velocity model that has been constructed by averaging the 1-D velocity models at 10 broadband stations (Fig. 1a), which are located



in the MCT zone, as obtained from the differential evolution waveform inversion of PRFs (“additional figures are given in Online Resource 1”). The apriori and final velocity models are shown in Fig. 1d. Both velocity models show a clear low-velocity layer at 10–20 km depth (Fig. 1d). This final model is used as the initial velocity model for our tomography. An excellent sampling of the study region by rays is seen from Fig. 2a–c, suggesting a good coverage for our local earthquake tomography study. We also determined a new 1-D velocity structure for the region through simultaneous inversion of 8412 P- and 8038 S- arrivals of 528 well-located events out of 913 earthquakes (Fig. 3a–c). The relocated earthquakes

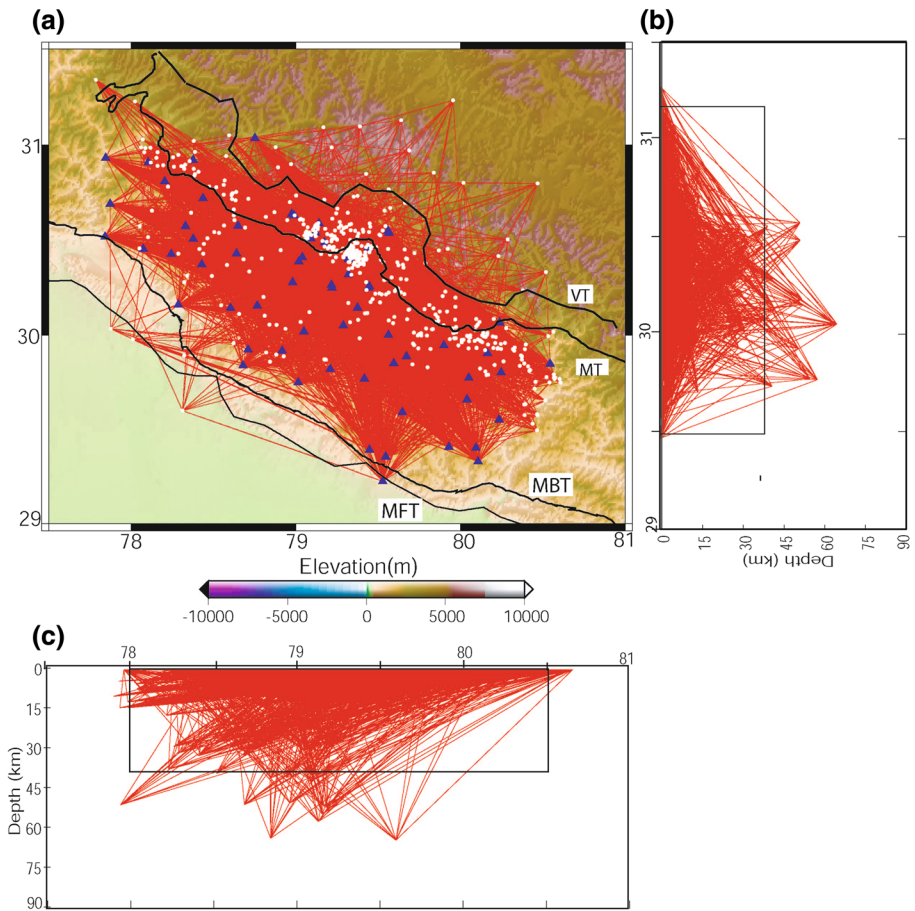


Fig. 2 **a** A plot showing ray sampling (red lines) of the study area for local earthquake velocity tomography. The inferred rupture zones of the 1803 (IRZ1) and 1505 (IRZ2) earthquakes are marked by solid thick dotted white lines (after Bilham (2019)). White dots mark epicentres, while blue filled triangles represent broadband seismograph stations, **b** N-S depth section of ray sampling (red lines) showing a good sampling of the crustal volume below the study area down to almost a depth of 35 km, and **c** E-W depth section of ray sampling (red lines) showing a good sampling of the crustal volume below the study area down to almost a depth of 35 km

are found to be occurring in the region just south of the MT (Fig. 3a-b) and very clearly delineate the main Himalayan thrust (MHT) that dips towards NE (Fig. 3b). For our tomographic inversion, the RMS residuals for P and S waves are reduced from 0.564 s to 0.284 s, and 0.547 s to 0.263 s, respectively, within 14 iterations (Fig. 3d-e). Note that our tomographic inversion is limited by 953 local earthquakes, which are spread over an area of 330 km × 330 km that might have resulted in poor resolution for some parts where number of earthquakes are less. Further, the focal depths of our events are there down to 35 km, which also results in a limitation to the resolving depth of tomograms. Thus, the results of our tomography would be reliable down to a depth of 35 km. Thus, if we use more number of events with focal depths deeper than 35 km then our tomograms will have better depth resolution down to the Moho depth, which would provide better insight into the structure

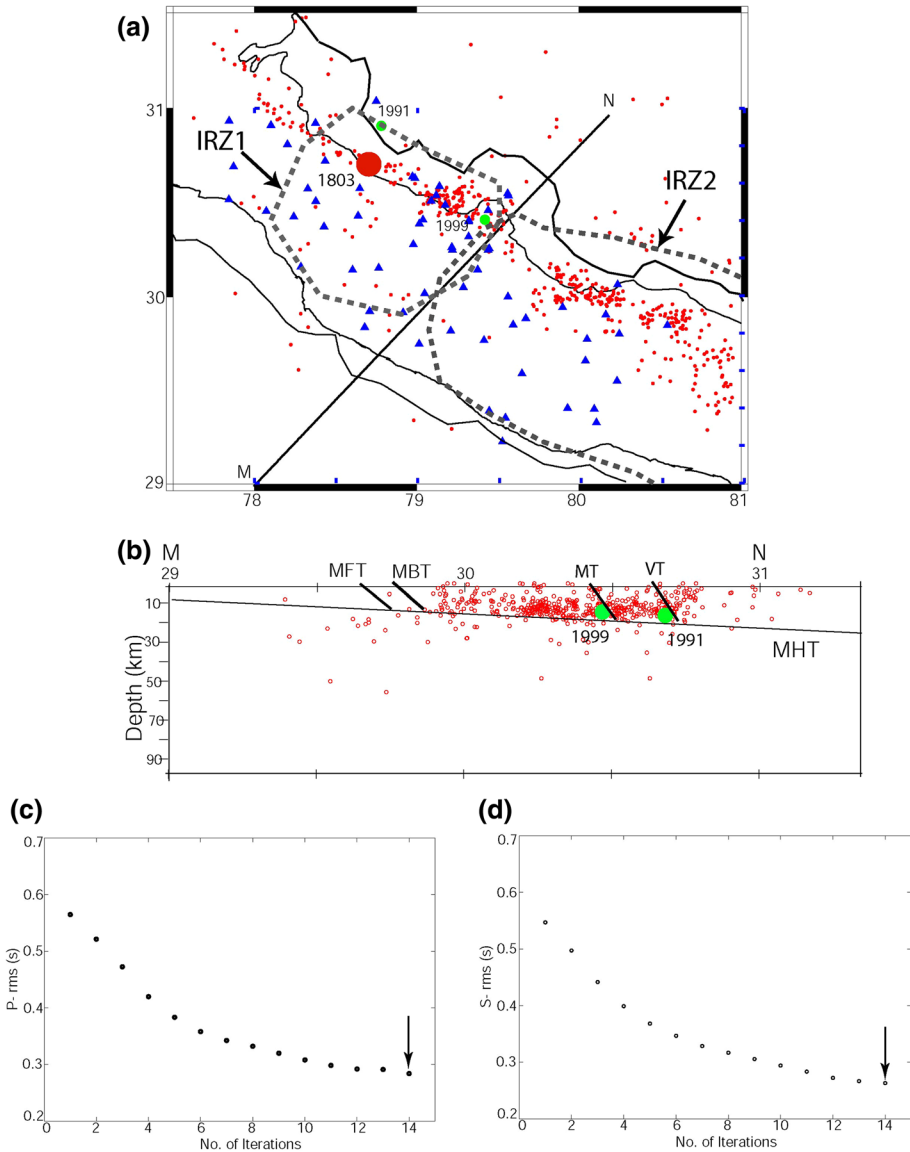


Fig. 3 **a** Earthquake relocations determined by simultaneous inversion are shown by small red circles. Three-component broadband seismographs mark by solid blue triangles. Two medium green filled circles represent the locations of the 1991 M_w 6.8 Uttarkashi and 1999 M_w 6.4 Chamoli earthquakes, while a large red filled circle marks the epicentral location of the 1803 event. The inferred rupture zones of the 1803 (IRZ1) and 1505 (IRZ2) earthquakes are marked by dotted thick white lines (after Bilham (2019)), **b** Depth cross section of relocated events across MN profile, showing seismicity along MHT and above it. However, some lower crustal and upper mantle earthquakes are also noticed. Red open circles mark the relocated earthquakes, while a black filled circle marks the hypocentre of the 1999 M_w 6.4 Chamoli event. RMS residual vs. number of iterations plots for **c** P- and **d** S- wave tomography. An arrow marks the minimum RMS value obtained at 14 iterations of the P- and S- tomography

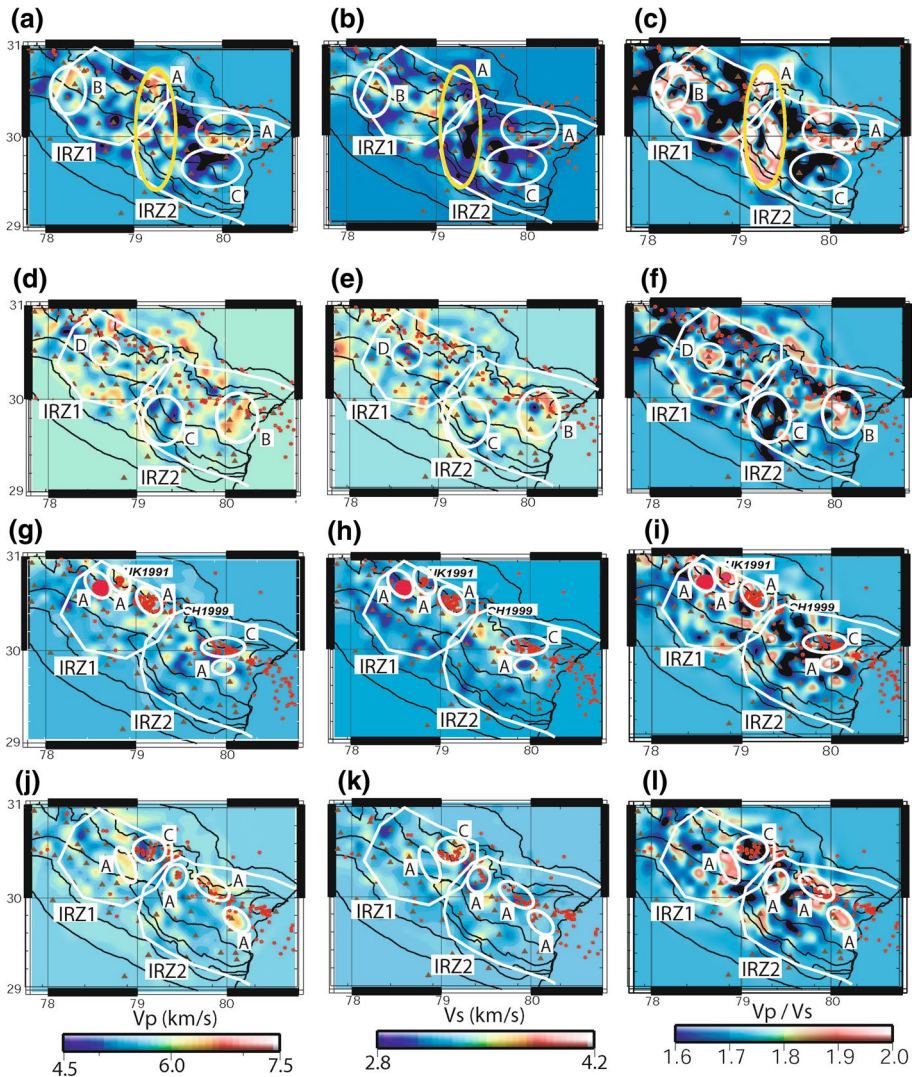


Fig. 4 Tomograms at 0–5 km depth, **a** V_p , **b** V_s and **c** V_p/V_s , tomograms at 5–10 km depth, **d** V_p , **e** V_s and **f** V_p/V_s , tomograms at 10–15 km depth, **g** V_p , **h** V_s and **i** V_p/V_s , and tomograms at 15–20 km depth, **j** V_p , **k** V_s and **l** V_p/V_s . Medium size red filled circles represent the epicentral locations of the 1991 M_w 6.6 Uttarkashi and 1999 M_w 6.4 Chamoli earthquakes, while small filled red circles mark relocations of events. A large red filled circle marks the location of the 1803 event. The inferred rupture zones of the 1803 (IRZ1) and 1505 (IRZ2) earthquakes are marked by solid thick white lines (after Bilham (2019)). Three-component broadband seismographs mark by solid brown triangles. White elliptical areas A, B, C and D mark zone of high fluid pressure (greater decrease in V_s than V_p with large V_p/V_s), mafic zone of low silica content (high V_p , moderate V_s and high V_p/V_s), zone of intermediate to high silica content (high V_p , low V_s and low V_p/V_s), and fluid-filled zone (low V_p , low V_s and high V_p/V_s), respectively. A large yellow elliptical zone marks an N-S trending transverse structure, which is associated with large fluid pressure

below the region. Further, if we have more number of events spatially well distributed over the whole region, then our tomograms would have better spatial resolution for the study region.

We use the tomographic inversion code developed by Benz et al. (1996) for our study. The modelling volume is discretized into 11,979 grid nodes, with the volume divided into $33 \times 33 \times 8$ nodes. A uniform horizontal grid spacing of 10 km and a vertical grid spacing of 5 km was considered in tomographic inversion whilst, for the computation of arrival times and ray tracing a uniform horizontal and vertical grid spacing of 1 km is used (“additional table is given in Online Resource 8”). The smoothing parameter decreases from 50 to 3 together with model roughness decreasing and not affecting the absolute velocities,

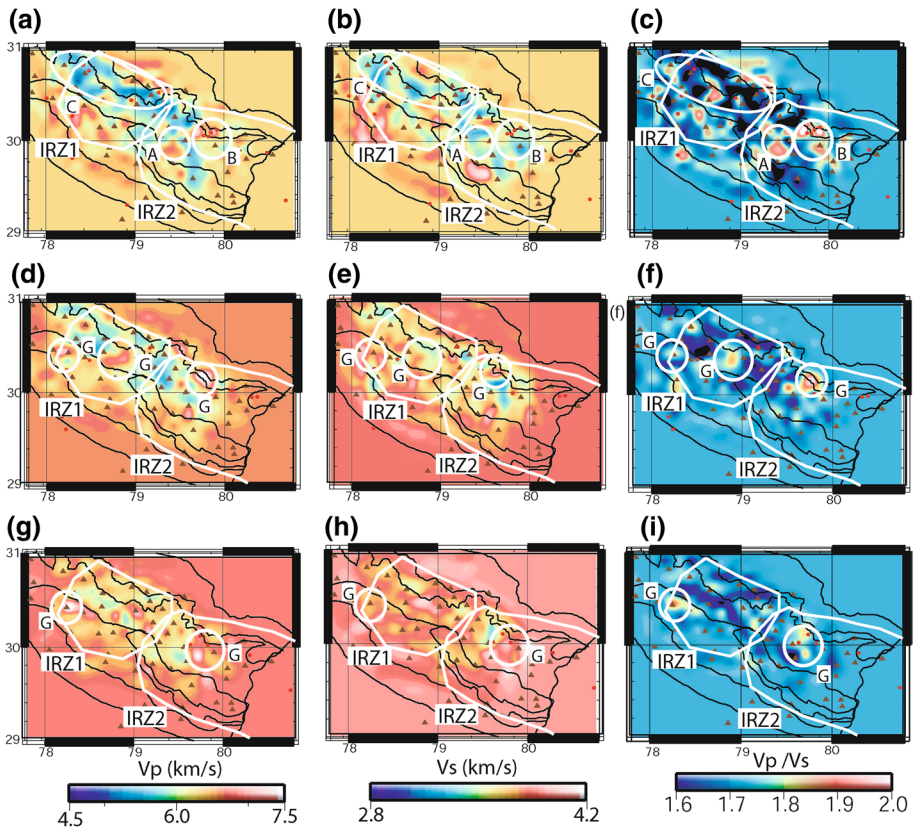


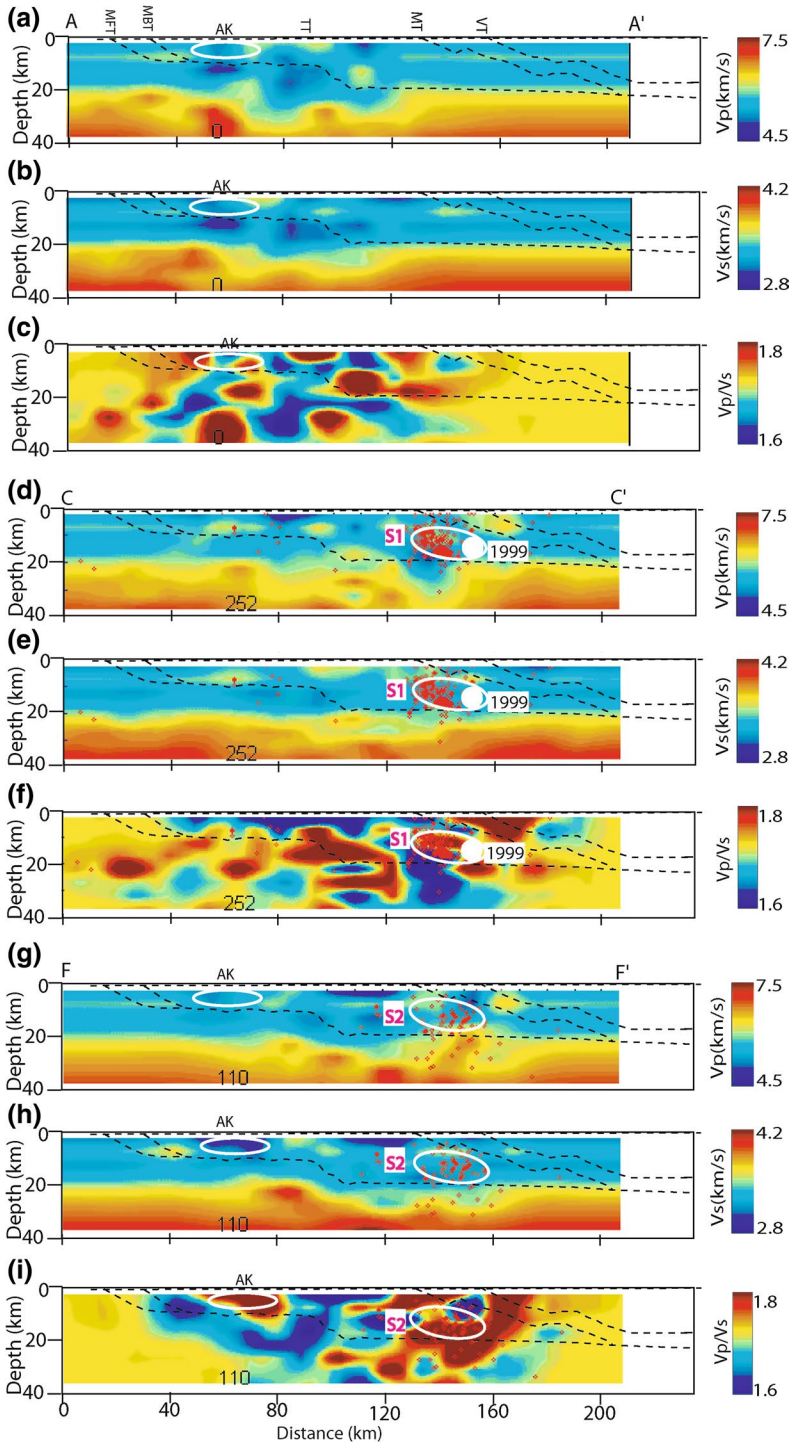
Fig. 5 Tomograms at 20–25 km depth, **a** V_p , **b** V_s and **c** V_p/V_s , tomograms at 25–30 km depth, **d** V_p , **e** V_s and **f** V_p/V_s , and tomograms at 30–35 km depth, **g** V_p , **h** V_s and **i** V_p/V_s . Medium size red filled circles represent the epicentral locations of the 1991 M_w 6.6 Uttarkashi and 1999 M_w 6.4 Chamoli earthquakes, while small filled red circles mark relocations of events. A large red filled circle marks the location of the 1803 event. The inferred rupture zones of the 1803 (IRZ1) and 1505 (IRZ2) earthquakes are marked by solid thick white lines (after Bilham (2019)). Three-component broadband seismographs mark by solid brown triangles. White elliptical areas A, B, and C mark zone of high fluid pressure (greater decrease in V_s than V_p with large V_p/V_s), mafic zone of low silica content (high V_p , moderate V_s and high V_p/V_s), and zone of intermediate to high silica content (high V_p , low V_s and low V_p/V_s), respectively, while white elliptical area G marks the presence of very high-velocity mafic granulite

Fig. 6 NE-SW depth cross sections of V_p , V_s and V_p/V_s along (a-c) Profile AA', (d-f) Profile CC', and (g-i) Profile FF'. Structural interpretation of the major thrusts in the Garhwal Himalaya is shown by grey dotted lines (from Srivastava and Mitra (1994)) projected into the line of our sections. Small red filled circles represent the hypocentral locations of earthquakes. Grey dotted lines mark the MHT zone. Large white circles represent the hypocentral locations of the 1999 M_w 6.4 Chamoli earthquake. The locations of these profiles are shown in Fig. 1a. S1 and S2 show white elliptical areas of low V_p , low V_s and high V_p/V_s values suggesting the presence of aqueous/metamorphic fluids. S1 is associated with a clustering of seismicity and the 1999 Chamoli event, while S2 is associated with a cluster of micro-earthquakes

the RMS residuals for P and S waves are reduced from 0.564 s to 0.284 s, and 0.547 s to 0.263 s, respectively, within 14 iterations (Fig. 3d-e). The depth slices of V_p , V_s and V_p/V_s tomograms from 0 to 35 km depths at 5 km depth interval are shown in Figs. 4–5, with depth cross sections along six NE-SW profiles (across the collisional zone) are shown in Fig. 6(a-i) and “additional figures are given in Online Resource 2”. Also, we constructed depth cross sections of V_p , V_s , and V_p/V_s tomograms along two NW–SE profiles to image the nature of crustal structure along the strike of the collisional zone in the Uttarakhand Himalaya (Fig. 7a-f). We also model differential V_p and V_s (i.e. final model–initial model) tomograms at 5 km interval between 0 and 35 km depth, which are shown in Figs. S3a-h, S4a-f. We also performed checkerboard test by assigning alternately high (+5%) and low-velocity (-5%) perturbations for individual grid nodes in 3-D, from 0 to 35 km depths at 5 km depth interval (Fig. 8a-h and “additional figures are given in Online Resources 5 and 6”). Our checkerboard test reveals a 90% retrieval of the V_p and V_s tomograms in the main seismogenic region, at 0–30 km depths (Fig. 8c-h and “additional figures are given in Online Resource 5”); however, only ~70–80% is retrieved for the remaining parts of the study area. Whilst at 30–40 km depths (“additional figures are given in Online Resource 6”), about ~75–85% of the velocity anomaly is retrieved within the central part, while only ~55–65% is retrieved for the rest.

4 Results and discussion

Analysis of depth slices for V_p , V_s and V_p/V_s tomograms at 0–5, 5–10, 10–15, 15–20, 20–25, 25–30, and 30–35 km depth ranges (Figs. 4a-l, 5a-i), reveal a laterally varying velocity structure across the inferred rupture zones of the 1803 (IRF1) and 1505 (IRZ2) great earthquakes in the KG Himalayan region comprising of several high and low-velocity anomalies. The high-velocity anomalies are characterized by a 10–20% increase in V_p and V_s and a 10% decrease in V_p/V_s values, which could be attributed to rigid and brittle crustal rocks, while the low-velocity anomalies are characterized by 10–20% decrease in V_p and V_s and a 10–14% decrease in V_p/V_s values, which could be representing fluid-filled zones. Our tomograms reveal on an average a lower velocity at 0–5 km depths in comparison to velocities at 5–10 km depths, which could be due to the presence of low strength, less rigid and weakly coupled sedimentary rocks that could be filled with meteoric water at 0–5 km depths. Most of the events at 0–5 km depths occur in the low-velocity zones, which could be triggered by the presence of crustal fluids, while some earthquakes are also noticed to occur in the high-velocity zones, which could be attributed to the seismic failure resulted from the large stress concentration associated with the brittle rigid competent high-velocity rocks. At 0–5 km depths, we also map an N-S trending transverse feature (characterized by high V_p , low V_s and high V_p/V_s values and marked by a yellow elliptical area in Fig. 4a-c) at the central zone between CRZ1 and CRZ2, which could be



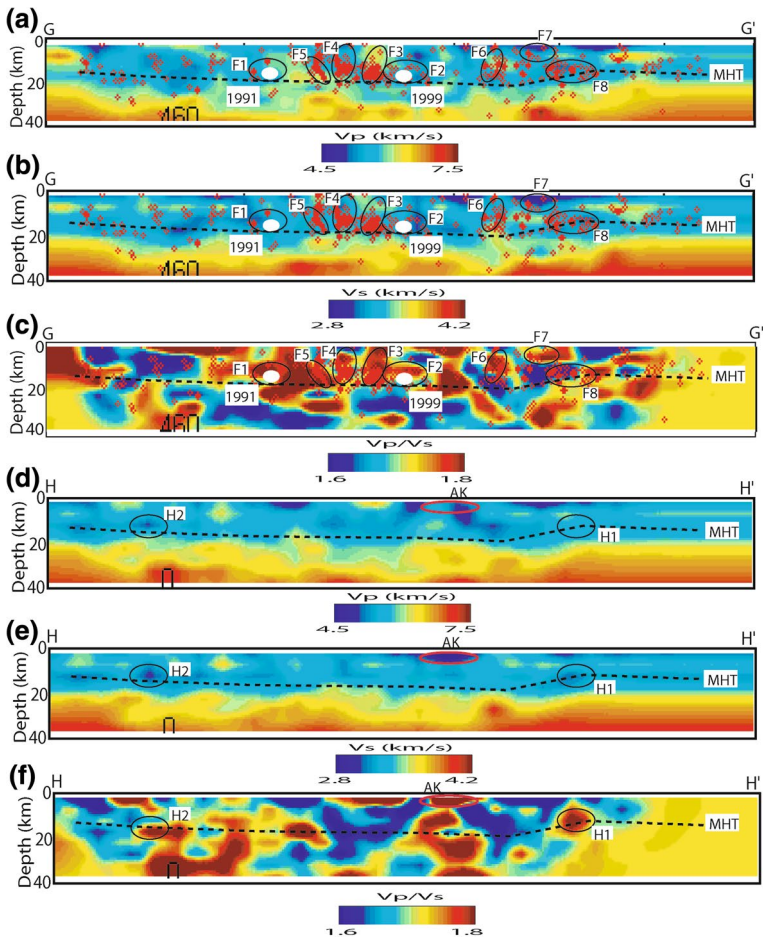


Fig. 7 V_p , V_s and V_p/V_s depth cross sections of V_p , V_s and V_p/V_s tomograms along **a**, **c**, and **e** GG' and **b**, **d**, **f** HH' profiles along the strike of the Himalayan collisional zone. Black elliptical areas F1, F3 and F5 are associated with high pore fluid pressure, while black elliptical areas F2, F4, F6 and F7 are associated with the presence of fluids. These elliptical areas are also associated with micro-earthquake clusters, while F1 and F2 are associated with the hypocentral locations of 1991 Uttarkashi and 1999 Chamoli events, respectively. Black dotted lines mark the main Himalayan thrust (MHT). Large filled white circles mark the 1991 Uttarkashi and 1999 Chamoli earthquakes, while relocated events are marked by small red circles. The locations of these profiles are shown in Fig. 1a

representing a permeable lithological contact with large fluid pressure. However, this transverse feature vanishes at depths deeper than 5 km (Fig. 4d-f). Based on the different nature of seismic velocities and V_p/V_s ratios we locate four zones viz., A, B, C and D shown by white elliptical areas in Fig. 4a-f. The zone A is characterized by greater decrease in V_s than V_p with large V_p/V_s , suggesting a zone of high fluid pressure, while zone B is characterized by high V_p , moderate V_s and high V_p/V_s , suggesting a mafic zone of low silica content, whereas high V_p , low V_s and low V_p/V_s characterize the zone -C, suggesting a zone of intermediate to high silica content, while zone-D is characterized by low V_p , low V_s and high V_p/V_s , representing a fluid-filled zone. The N-S trending transverse

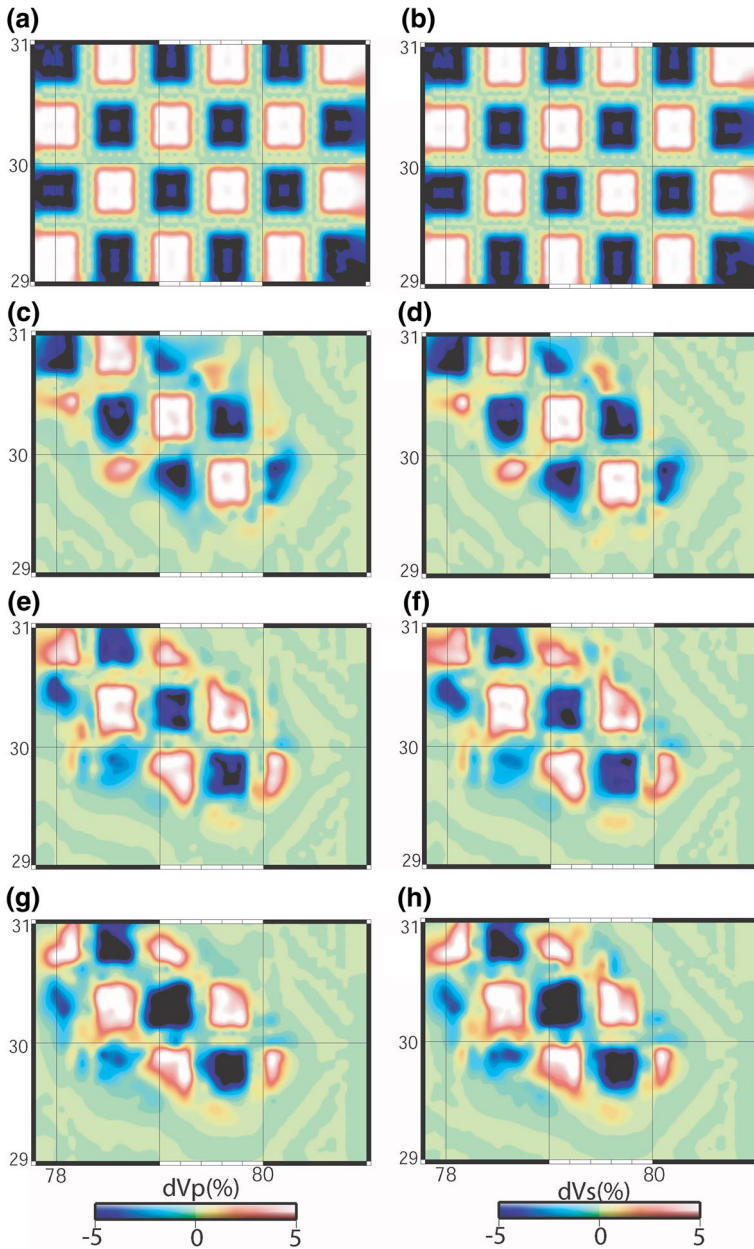


Fig. 8 Results of Checkerboard test. **a, b** Input perturbation model, consisting of 330 km³ with velocities 5% compared to the starting model for P- and S- waves, **c, d** recovered perturbation models for P- and S- waves at 5–10 km depths, **e, f** recovered perturbation models for P- and S- waves at 15–20 km depths, and **g, h** recovered perturbation models for P- and S- waves at 25–30 km depths. Broadband stations are marked by filled brown triangles, while locations of the 1991 Uttarkashi and 1999 Chamoli earthquakes are shown by red filled circles

structure (marked by a large yellow elliptical area in Fig. 4a–f) is also marked as zone A, which is inferred to be associated with large fluid pressure. These A, B, C and D zones are also mapped in tomograms at 10–15 km, 15–20 km and 20–25 km depths (Figs. 4g–i, 5a–c). However, these zones are not mapped at 25–35 km depths. Rather, zone-G is mapped at 25–35 km depths, which is characterized by very high Vp (> 7.0 km/s), very high Vs (> 3.9 km/s) and very high Vp/Vs (> 1.85), representing rocks with mafic granulite composition (Christensen and Mooney 1995).

We also notice low-velocity anomalies at 5–35 km depths, which might be attributed to the zones filled with aqueous or metamorphic fluids. Whilst high-velocity zones at 5–35 km depths could be attributed to the presence of high strength rigid and strongly coupled rocks that could accumulate large strain energy due the ongoing convergence (Bilham 2019; Ader et al. 2012). Interestingly, we notice marked lateral variations in seismic velocities (Vp, Vs and Vp/Vs) across the rupture zones of both 1803 and 1505 events at 0–25 km depths (Figs. 4a–l and 5a–c), suggesting a marked laterally varying structural heterogeneities. However, this high level of lateral variations in seismic velocities is noticed to be reduced at 25–35 km depths (Fig. 5d–i). We also observe that the nature of velocity anomalies changes with increasing depth and becomes dominant with lower velocity anomalies (Vp: 5.3–6.2 km/s; Vs: 2.8–3.7 km/s; Vp/Vs: 1.7–2.1) between 10 and 20 km. Interestingly, the detachment plane (i.e. main Himalayan thrust (MHT)) coincides with this low-velocity zone. Majority of earthquakes also occur between 10 and 20 km depth below the MCT zone, which is modelled to be characterized by low to moderate Vp and Vs and high Vp/Vs ratio (~ 1.8 –2.1), representing zones filled with aqueous/metamorphic fluids probably resulting from the metamorphic dehydration reaction due to the under-thrusting Indian crust^{26,29}. Our tomograms also show several high-velocity anomalies within the MHT zone representing high strength rigid and strongly coupled rocks at 5–20 km depths, which can accumulate large strains due to the continued northward Himalayan convergence (Pei et al. 2016). It is observed that the 1803 M_w 8.2 (Bilham et al. 2019), 1991 M_w 6.8 Uttarkashi (Cotton et al. 1996) and 1999 M_w 6.4 Chamoli (Mandal et al. 2001) earthquakes have occurred between 10 and 15 km depth in the low-velocity zones on the MHT (Figs. 4–5). Thus, it can be inferred that stress loading in the high-velocity rigid rocks within the MHT might be accumulating large stresses due to the continued northward Himalayan convergence, which subsequently led to the generation of earthquakes due to crustal fluid flows (low-velocity zones). Therefore, earthquakes associated with the low-velocity MHT could be inferred as the fluid-triggered earthquakes. However, in contrast, higher velocities characterize the whole region between 20 and 35 km depths (Fig. 5a–f). Below the Askot Klippe (AsK) and Chiplakot crystalline belt (CCB) in the eastern side of the study area, both Vp and Vs tomograms are laden with high-velocity anomalies (with low Vp/Vs) between 5 and 35 km depths except the dominant low-velocity anomaly (with high Vp/Vs) between 10 and 20 km depth coinciding with the MHT (Figs. 1a, 5a–f). Two other high-velocity anomalies between 20 and 35 km depths are also noticed, which are located below the Lansdowne Klippe (LK) and Almora Klippe (AK) (Figs. 1a, 5a–f). These high-velocity anomalies associated with the Askot Klippe (AsK) and Chiplakot crystalline belt (CCB) could be attributed to the mafic higher Himalayan rocks, while the low-velocity anomalies below the Lansdowne Klippe (LK) and Almora Klippe (AK) could be attributed to the exhumation and sediments associated with these Klippes (Patel et al. 2020).

We notice a domination of higher Vp and Vs (with low Vp/Vs ratio) between 20 and 35 km depth, suggesting the presence of rigid mafic lower crustal rocks (Fig. 5a–i). At 20–30 km depths, we also notice an NW–SE trending large area of low velocity (low Vp: 5.8–6.1 km/s, low Vs: 3.4–3.6 km/s; low Vp/Vs: 1.6–1.8), suggesting the presence

of rocks with intermediate to high silica content (Musacchio et al. 1997). Most interestingly, our tomograms clearly image some NNE-NS trending anomalies with very high Vp (> 7.5 km/s), high Vs (> 4.2 km/s) and low Vp/Vs (~ 1.6) between 25 and 35 km depth (shown by white elliptical areas in Fig. 5d–i), which might be representing very rigid and competent lower crustal rocks with a composition similar to the granulite (Christensen and Mooney 1995). These high-velocity anomalies are not seen at shallower depths down to 25 km (Figs. 4a–l and 5a–c). If we compute density from Vp, then these high-velocity rocks have a very high-density value of the order of ~ 3.0 – 3.4 gm/cm³ that might be representing a mafic granulitic layer (initial stage of the partial eclogitization), which might be representing the subducted Indian lower crustal rocks as also suggested by Hatzfeld and Molnar (2010). Note that Patel et al. (2020) have reported occurrences of mafic xenoliths/granulite from the Kailash Kinnaur granite that is located just 50–60 km west of our study area. It would be worth mentioning here that evidence of lower crustal eclogitization has already been reported below the Tibetan Himalaya (Schulte-Pelkum et al. 2005), which is located further north of our study region.

We also calculate differential Vp and Vs tomograms at 5 km depth interval between 0 and 35 km, by subtracting initial 3-D velocity model from the final tomograms (“additional figures are given in Online Resources 4 and 5”). Our differential tomograms show high-velocity anomalies (10–20% increase in Vp and Vs) down to 25 km depth, but these high-velocity anomalies are not mapped between 25 and 35 km depths. Thus, our differential tomograms reveal a highly deformed and heterogeneous upper crust (0–25 km depth) and a less deformed and relatively homogeneous lower crust (25–35 km depth), suggesting the fact that deformations due to the continued northward Himalayan convergence are mainly accommodated with the upper crustal layers down to 25 km depth, which is in a good agreement with the findings of GPS studies in the Himalaya (Ader et al. 2012). Our differential Vp and Vs tomograms between 25 and 35 km depths (“additional figures are given in Online Resource 3”) are mainly dominated by low-velocity anomalies (10–15% reduction in Vp and Vs). This kind of low-velocity anomalies supports the idea of the presence of relatively higher temperature and lower strength, which results in ductile rheology of the lower crust (Xu et al. 2007), which can also explain the lack of earthquakes in the lower crust in this actively deforming region.

To map the MHT, we analyse depth cross sections of Vp, Vs and Vp/Vs tomograms along six NE-SW profiles (across the strike of the collisional zone) (Fig. 6a–i and “additional figures are given in Online Resource 2”). These cross sections distinctly map a shallow north-dipping low-velocity zone (Vp: 4.4–5.7 km/s; Vs: 2.8–3.3 km/s; Vp/Vs: 1.6–1.7) at 10–20 km depths, which is defined here as the MHT (marked by grey dotted lines in Fig. 6a–i and “additional figures are given in Online Resource 2”). Most of the micro-earthquakes (including the 1999 Chamoli earthquake) have noticed to occur within the low-velocity patches (with high Vp/Vs ratio ($\sim > 1.8$)) within the MHT zone (marked by white elliptical areas S1 in Fig. 6d–f and S2 in Fig. 6g–i). Thus, we infer that these earthquakes on the MHT might have been triggered by the presence of aqueous/metamorphic fluids or high pore fluid pressure (Caldwell et al. 2013; Bai et al. 2019; Monsalve et al. 2006; Mahesh et al. 2013), while some earthquakes are observed to occur in the low-velocity patches (with a low Vp/Vs ratio (~ 1.6 – 1.7)) within the MHT, which could be triggered by accumulation of large stresses associated with the rocks with intermediate to high silica content (Musacchio et al. 1997). We also image a few zones of low Vp, low Vs and larger Vp/Vs ratios at 5–30 km depths, which could be attributed to the fluid-filled (aqueous/metamorphic fluids) crustal zones (Fig. 6a–i and “additional figures are given in Online Resource 1”). Magneto-telluric studies in Uttarakhand and Nepal Himalaya have mapped

high conductivity zone in the depth range between 10 and 20 km, and is interpreted as the presence of aqueous fluids (Lemonnier et al. 1999; Rawat et al. 2014). Alternatively, low conductivity (low velocity) zones could also be explained in terms of the presence of graphitic schists (Jones et al. 2005). We also notice across all the NE-SW profiles (Fig. 6a–i and “additional figures are given in Online Resource 1”) that the MHT is associated with low velocity (Vp: 4.4–5.7 km/s; Vs: 2.8–3.3 km/s) and low Vp/Vs (~1.6–1.7) anomalies, which could be attributed to the presence of aqueous fluids with high pore pressure in the MHT Zone resulting in the generation of fluid-triggered earthquakes (Bai et al. 2019; Monsalve et al. 2006; Mahesh et al. 2013).

4.1 Possible earthquake generation model in the Kumaon–Garhwal Himalaya

To understand the seismo-genesis of earthquakes, we also construct depth cross sections of Vp, Vs and Vp/Vs along two WNW-ESE trending (along the strike of the Himalayan collisional zone) GG' and HH' profiles (Fig. 1a). These cross sections (Fig. 7a–f) clearly image marked lateral variations and presence of structural heterogeneities across the whole Kumaon–Garhwal Himalaya. Along the GG' cross section (Fig. 7a–c), we also notice some black elliptical areas (viz., F1, F3, F5 and F8), which are observed to be characterized by greater decrease in Vs than Vp with large Vp/Vs, suggesting a zone of high pore-fluid pressure, while some black elliptical areas (viz., F2, F4, F6 and F7) along the GG' cross section (Fig. 7a–c) are observed to be characterized by low Vp, low Vs and high Vp/Vs, suggesting zones filled with aqueous/metamorphic fluids. These elliptical areas are also associated with upper crustal micro-earthquake clusters, suggesting occurrences of these earthquakes due to presence of fluids or high pore-fluid pressure. Elliptical areas F1 and F2 are found to be associated with the hypocentral locations of the 1991 Uttarkashi and 1999 Chamoli events, respectively. Thus, we infer that both the 1991 Uttarkashi and 1999 Chamoli earthquakes were triggered by high pore fluid pressure (resulting from the presence of aqueous or metamorphic fluids) within the MHT. Along the HH' cross section, we notice lack of seismicity correlating well with the less permeable upper crust with smaller Vp/Vs values (Fig. 7d–f). A red elliptical area (characterized by low Vp, low Vs and high Vp/Vs) at 0–5 km depths along the HH' cross section marks the location of Almora klippe (AK) is marked by, which is inferred to be fluid-filled (meteoric water saturated sediments). We also notice black elliptical area H1 (characterized by greater decrease in Vs than Vp with large Vp/Vs, suggesting a zone of high pore-fluid pressure) and H2 (characterized by low Vp, low Vs and high Vp/Vs, suggesting zones filled with aqueous/metamorphic fluids) along the HH' cross section (Fig. 7d–f).

Our study reveals a MHT (at 10–20 km depth) that dips towards NE at a shallow angle of 1–2° (Fig. 3b). The focal depths of the 1991 Uttarkashi and 1999 Chamoli earthquakes are reported to be 16 and 15 km, respectively (Bilham, 2019; Harbindu et al. 2012). We calculate static frictional coefficient (i.e. the ratio between shear stress and normal stress) in the MHT at 15 km depth. Following Turcotte and Schubert (2002), we calculate the shear and normal (σ_n) stresses using following relations $\sigma_n = \rho gz + (\Delta\sigma_{xx}/2) (1 + \cos 2\theta)$ and $\tau = -(\Delta\sigma_{xx}/2) \sin 2\theta$ where ρ is the density, “ $\Delta\sigma_{xx}$ ” is the horizontal deviatoric stress, and “ θ ” is the angle between the MHT and the vertical. The reported stress drops of the 1991 UK and 1999 CH earthquakes are 3.3 and 10.5 MPa (Harbindu et al. 2012), respectively, suggesting lower bounds on the pre-earthquake shear stress on the MHT, averaged over the rupture. Thus, assuming $\tau = 10.5$ MPa, we model the static frictional coefficient (μ) of 0.08 on the shallow (~2°) NE dipping MHT at 15 km depth. However, if we assume

$\tau = 3.3$ MPa, then modelled μ at 15 km depth is modelled to be 0.01. Our modelled μ at 15 km depth, which varies from 0.01 to 0.08, agree well with the reported values from other research investigations of the Himalayan area (Herman et al. 2010; Copley et al. 2011). Such a low frictional coefficient in the MHT could be attributed to the presence of clay minerals or fluids (Copley et al. 2011). Note that Herman et al. (2010) and Copley et al. (2011) have also modelled a friction coefficient of 0.07 and 0.08 for the MHT, respectively. It would be worth to mention here that Copley et al. (2011) modelled $\mu = 0.08$ within the MHT between 5 and 25 km depth for the Ganges basin. The low μ values could be attributed to the highly fractured and fluid-filled MHT zone, which has been resulted from the continued convergence between Indian and Eurasian plates. Since the MHT is highly fractured, thus, less shear stress would be required to generate an earthquake. Further, the presence of fluids resulting in the high pore fluid pressure would further facilitate the generation of earthquakes within the MHT zone.

Most interestingly, our modelling reveals that all three large and great past earthquakes (viz., the 1803 M_w 8.2 Garhwal, 1991 M_w 6.8 Uttarkashi and 1999 M_w 6.4 Chamoli) and present micro-earthquake activity have occurred in the zones within the MHT between 10 and 20 km depths, which are characterized by low V_p , low V_s and high V_p/V_s (Fig. 6a–i and “additional figures are given in Online Resource 1”). Thus, we can infer that these past earthquakes might have been triggered by either the presence of aqueous/metamorphic fluids or high pore-fluid pressure within the MHT. Based on the above-discussed criteria, we detect three similar locales S2, B1 and E1, which are shown by white elliptical areas with the micro-earthquake clustering between 10 and 20 km depths, along FF’, BB’ and EE’ profiles, respectively (Fig. 6a–i and “additional figures are given in Online Resource 1”). Therefore, two probable un-ruptured zones (viz., S2 and E1) for future earthquakes are detected in the rupture zone of the 1505 great earthquake, while one future un-ruptured locale (i.e. B1) is detected in the rupture zone of the 1803 great event. Thus, our study suggests that the un-ruptured zones in the rupture zone of 1505 great earthquake are having more hazard related to the occurrences of moderate to large earthquakes in the KG Himalaya in comparison to the rupture zone of 1803 event. Besides, another similar locale (D1) is detected in the rupture zone of the 1505 earthquake along the profile DD’, which is shown by a white elliptical area with micro-earthquake activity between 10 and 20 km depths (“additional figures are given in Online Resource 1”). But, D1 is characterized by low V_p , low V_s and low V_p/V_s , suggesting intermediate to high silica content and may not be very favourable for nucleating moderate to large earthquakes in future. The above-discussed three predicted un-ruptured zones (i.e. B2, S2 and E1) are mainly characterized by the presence of aqueous or metamorphic fluids or high pore-fluid pressure, which are surrounded by or sandwiched between high-velocity zones (i.e. high strength and strongly coupled rocks) and can act as strain accumulators due to the continued northward Himalayan convergence (Figs. 4, 5, 6 and “additional figures are given in Online Resource 2”). Therefore, we infer that these three mapped unruptured zones could be the most probable zone for the future fluid-triggered moderate to large earthquakes on the MHT in the KG Himalaya.

5 Conclusions

The tomographic inversion is performed here using 14,074 P- and 13,013 S- arrival times of 913 local earthquakes of ML0.8–5.5 from a dense network of 65 seismic stations, which provides three-dimensional P- and S- wave velocity models of the Uttarakhand Himalaya down to a depth of 35 km. Our modelling provides new constraints on the lateral seismic velocity (V_p , V_s and V_p/V_s) variations across the inferred rupture zones of the Mw8.2 1505 and Mw8.0 1803 great earthquakes in the Kumaon–Garhwal Himalaya. Our modelling clearly delineates low-velocity sedimentary layers of the overriding Eurasian plate and a high-velocity under-thrust Indian crust below the region. Seismic velocity tomograms delineate a shallow ($1\text{--}2^\circ$) NE dipping low velocity (V_p : 4.5–5.7 km/s; V_s : 2.8–3.3 km/s; V_p/V_s : 1.6–1.7) MHT zone extending from 10 to 20 km depth. The observed low-velocity anomaly could be attributed to the presence of aqueous or metamorphic fluids and high fluid pressure within the MHT zone. Thus, the high fluid pressure along with the inferred low frictional coefficient ($\sim 0.01\text{--}0.08$) might be triggering small to large earthquakes on the MHT. Based on modelled V_p , V_s and V_p/V_s tomograms, our study detects several pockets of different lithological formations at different upper crustal (0–25 km depths) (viz., aqueous/metamorphic fluid-filled zones, high pore-fluid pressure zones, zones with intermediate to high silica content, mafic zones with less silica content) and lower crustal (25–35 km depths) (viz., zones with rocks of granulite composition).

The main finding of our modelling is the detection of low-velocity anomalies associated with the hypocentral zones of the 1803 M_w 8.2 Garhwal, 1991 M_w 6.8 Uttarkashi and 1999 M_w 6.4 Chamoli earthquakes. These low-velocity anomalies are inferred to be associated with the zones filled with aqueous/metamorphic fluids or high pore fluid pressure within the MHT at 10–20 km depths. Thus, we infer that these past earthquakes might have been triggered by either the presence of aqueous/metamorphic fluids or high pore-fluid pressure within the MHT. We also detect three unruptured similar locales in the region, which are characterized by low velocity (low V_p , low V_s and high V_p/V_s) anomalies between 10 and 20 km depths. These predicted locales are also found to be surrounded by or sandwiched between high-velocity zones (i.e. high strength and strongly coupled rocks). Thus, these high-velocity zones can act as strain accumulators due to the continued northward Himalayan convergence. Therefore, these three mapped locales could be the most probable zones for the generation of future fluid-triggered moderate to large earthquakes on the MHT in the KG Himalaya. Two out of three predicted locales are lying in the western part of the rupture zone of the 1505 great earthquake, which probably qualifies this part to be relatively more vulnerable to the generation of future moderate to large earthquakes in comparison to the rupture zone of the 1803 event.

Supplementary Information The online version contains supplementary material available at <https://doi.org/10.1007/s11069-021-05135-4>.

Acknowledgements Authors are grateful to the Director, Council of Scientific and Industrial Research—National Geophysical Research Institute (CSIR-NGRI), Hyderabad, India, for his support and permission to publish this work. Figures were plotted using the Generic Mapping Tool (GMT) software (Wessel et al. 2013). This study was supported by the CSIR-NGRI, Hyderabad, India. The current seismic network in the Kumaon–Garhwal Himalayan region is operated under a Mission-Mode Project (HCP0017) project supported by the CSIR-NGRI. Datasets for this research are included in this paper and its supplementary material. We dedicate this paper to our colleague late Mr. YVVBSN Murthy, who generated the basic phase data of precise P- and S- arrival times for our tomographic study.

Declarations

Conflict of interest The authors declared that there is no conflict of interest.

Data availability Datasets for the present study are included in this paper and its supplementary information files. The P- and S- arrival times, earthquake location, and station location data used in the present work can be obtained from the https://www.ngri.org.in/84567952/uk_tomo.zip.

References

- Ader T, Avouac J-P, Liu-Zeng J, Lyon-Caen H, Bollinger L, Galetzka J, Genrich J, Thomas M, Chanard K, Sapkota SN, Rajaure S, Shrestha P, Ding L, Flouzat M (2012) Convergence rate across the Nepal Himalaya and interseismic coupling on the Main Himalayan Thrust: Implications for seismic hazard. *J Geophys Res.* <https://doi.org/10.1029/2011JB009071>
- Bai L, Klemperer SL, Mori J, Karplus MS, Ding L, Liu D, Li G, Song B, Dhakal S (2019) Lateral variation of the main himalayan thrust controls the rupture length of the 2015 Gorkha earthquake in Nepal. *Sci Adv* 5(eaav0723):1–7
- Benz HM, Chouet BA, Dawson PB, Lahr JC, Page RA, Hole JA (1996) Three dimensional P and S wave velocity structure of Redoubt Volcano, Alaska. *J Geophys Res* 101:8111–8128
- Bilham R (2019) Himalayan earthquakes: a review of historical seismicity and early 21st century slip potential. *Geol Soc Lond Spec Publ* 483:423–482
- Caldwell WB, Klemperer SL, Lawrence JF, Rai SS, Ashis, (2013) Characterizing the main himalayan thrust in the Garhwal Himalaya, India with receiver function CCP stacking. *EPSL* 367:15–27
- Christensen NI, Mooney WD (1995) Seismic velocity structure and composition of the continental crust: a global view. *J Geophys Res* 100(B6):9761–9788
- Copley A, Avouac J-P, Hollingsworth J, Leprince S (2011) The 2001 Mw 7.6 Bhuj earthquake, low fault friction, and the crustal support of plate driving forces in India. *J Geophys Res.* <https://doi.org/10.1029/2010JB008137>
- Cotton F, Campillo M, Deschamps A, Rastogi BK (1996) Rupture history and seismotectonics of the 1991 Uttarkashi, Himalaya earthquake. *Tectonophysics* 258:35–51
- Drukpa D, Velasco AA, Doser DI (2006) Seismicity in the Kingdom of Bhutan (1937–2003): Evidence for crustal transcurrent deformation. *J Geophys Res* 111:B06301. <https://doi.org/10.1029/2004JB008137>
- Elliott JR, Jolivet R, González PJ, Avouac J-P, Hollingsworth J, Searle MP, Stevens VL (2016) Himalayan megathrust geometry and relation to topography revealed by the Gorkha earthquake. *Nature Geosci* 9:174–180. <https://doi.org/10.1038/ngeo2623>
- Gupta H, Gahalaut VK (2014) Seismotectonics and large earthquake generation in the Himalayan region. *Gondwana Res* 25:204–213
- Harbindu A, Sharma ML (2012) Stochastic ground-motion simulation of two Himalayan earthquakes: seismic hazard assessment perspective. *J Seismology* 16:345–369
- Hatzfeld D, Molnar P (2010) Comparisons of the Kinematics and deep structures of the Zagros and Himalaya and of the Iranian and Tibetan plateaus and geodynamics implications. *Rev Geophys* 48:1–48
- Herman F et al (2010) Exhumation, crustal deformation, and thermal structure of the Nepal Himalaya derived from the inversion of thermos-chronological and thermos-barametric data and modeling of the topography. *J Geophys Res* 115:B06407. <https://doi.org/10.1029/2008JB006126>
- Jones AG, Ledo J, Ferguson IJ (2005) Electromagnetic images of the Trans-Hudson orogen: the North American Central Plains anomaly revealed. *Can J Earth Sci* 42:457–478
- Joshi M, Kothiyari GC, Ahluvalia A, Pant PD (2010) Neotectonic evidences of rejuvenation in Kaurik-Chango Fault Zone, Northwestern Himalaya. *J Geogr Inf Syst* 2:169–176
- Kayal JR, Ram S, Singh OP, Chakraborty PK, Krunakar G (2003) Aftershock of the 1999 Chamoli earthquake and seismotectonic structure of the Garhwal Himalaya. *Bull Seismol Soc Am* 93:109–117
- Kumar N, Sharma J, Arora BR, Mukopadhyay S (2009) Seismotectonic model of the Kangra-Chamba sector of Northwest Himalaya: Constraints from joint hypocenter determination and focal mechanism. *Bull Seismol Soc Am* 99:95–109
- Langin W, Brown L, Sandvol E (2003) Seismicity in central Tibet from project INDEPTH III seismic recordings. *Bull Seism Soc Am* 93:2146–2159

- Lemonnier C, Marquis G, Perrier F, Avouac J-P, Chitrakar G, Kafle B, Sapkota S, Gautam U, Tiwari D, Bano M (1999) Electrical structure of the Himalaya of central Nepal: high conductivity around the mid-crustal ramp along the MHT. *Geophys Res Lett* 26:3261–3264
- Mahesh P, Rai SS, Sivaram K, Paul A, Gupta S, Sarma R, Gaur VK (2013) One dimensional reference velocity model and precise locations of earthquake hypocenters in the Kumaon-Garhwal Himalaya. *Bull Seism Soc Am* 103:328–339
- Mandal P, Padhy S, Rastogi BK, Kousalya M, Satyanarayana HVS, Satyamurthy C, Vijayaraghavan R, Srinivasan A (2001) Aftershock activity and low coda Q_c in the epicentral region of the 1999 Chamoli earthquake of M_w 6.4. *Pure Appl Geophys* 158:1719–1735
- Molnar P, Lyon-Caen H (1989) Fault plane solutions of earthquakes and active tectonics of the Tibetan Plateau and its margins. *Geophys J Int* 99:123–153
- Monsalve G, Sheehan A, Schulte-Pelkum V, Rajaure S, Pandey MR, Wu F (2006) Seismicity and one-dimensional velocity structure of the Himalayan collision zone: earthquakes in the crust and upper mantle. *J Geophys Res* 111:B10301. <https://doi.org/10.1029/2005JB004062>
- Musacchio G, Mooney WD, Luetgert JH (1997) Composition of the crust in the Grenville and Appalachian Provinces of North America inferred from V_p/V_s ratios. *J Geophys Res* 102:15225–15241
- Ni J, Barazangi M (1984) Seismotectonics of the Himalayan collisional zone: geometry of the underthrusting Indian plate beneath the Himalaya. *J Geophys Res* 89(B2):1147–1163
- Pandey MR, Tandukar RP, Avouac JP, Lavé J, Massot JP (1995) Evidence for recent interseismic strain accumulation on a mid-crustal ramp in the central Himalaya of Nepal. *Geophys Res Lett* 22:751–758. <https://doi.org/10.1029/94GL02971>
- Patel RC, Manmohan KR, Kumar R (2020) Tectonic control on exhumation and seismicity in the Garhwal-Kumaun Himalaya, NW-India. *Terra Nova* 32:23–33
- Pei S, Liu H, Bai L, Liu Y, Sun Q (2016) High-resolution seismic tomography of the 2015 M_w 7.8 Gorkha earthquake, Nepal: evidence for the crustal tearing of the Himalayan rift. *Geophys Res Lett* 43:9045–9052
- Rajendran CP, Rajendran K (2005) The status of central seismic gap: a perspective based on the spatial and temporal aspects of the large Himalayan earthquakes. *Tectonophysics* 395:19–39
- Rawat G, Arora BR, Gupta PK (2014) Electrical resistivity cross-section across the Garhwal Himalaya: Proxy to fluid seismicity linkage. *Tectonophysics* 637:68–79
- Schulte-Pelkum V, Monsalve G, Sheehan A, Pandey MR, Sapkota S, Bilham R, Wu F (2005) Imaging the Indian subcontinent beneath the Himalaya. *Nature* 435:1222–1225
- Seeber L, Armbruster J (1981) Great detachment earthquakes along the Himalayan Arc and long-term forecasting, in *Earthquake Prediction: An International Review*, Maurice Ewing Ser., vol. 4, edited by D. W. Simpson and P. G. Richards, pp. 259–277, AGU, Washington, D. C.
- Srivastava P, Mitra G (1994) Thrust geometries and deep structure of the outer and lesser Himalaya, Kumaon and Garhwal (India): implications for evolution of the Himalayan fold-and-thrust belt. *Tectonics* 13:89–109
- Turcotte DL, Schubert G (2002) *Geodynamics*, 2nd edn. Cambridge Univ. Press, Cambridge
- Valdiya KS (1980) *Geology of the Kumaon Lesser Himalaya*, 291 pp., Wadia Inst. of Himalayan Geol., Dehra Dun, India
- Vorobieva I, Mandal P, Gorshkov A (2017) Block-and-fault dynamics modelling of the Himalayan frontal arc: implications for seismic cycle, slip deficit, and great earthquakes. *J Asian Earth-Sci* 148:131–141
- Wessel P, Smith WHF, Scharroo R, Luis JF, Wobbe F (2013) Generic mapping tools: improved version released. *EOS Trans AGU* 94:409–410